The International Journal of Advanced Manufacturing Technology (2022) 122:2361–2378
https://doi.org/10.1007/s00170-022-10012-w

ORIGINAL ARTICLE

Simultaneous effects of cutting depth and tool overhang on the vibration behavior of cutting tool and high-cycle fatigue behavior of product: experimental research on the turning machine

Dmitry Gennadievich Allenov[1] · Kristina Deinova Borisovna[1] · Siamak Ghorbani[1] · Kazem Reza Kashyzadeh[2,3]

Received: 19 April 2022 / Accepted: 19 August 2022 / Published online: 1 September 2022

Abstract
One of the major challenges in the manufacturing parts, especially metals, is turning with good/excellent surface quality, which has a significant effect on the fatigue strength of the industrial components. Selecting incorrect or unsuitable values of machining parameters leads to vibration instability in the cutting tool and as a result, excessive roughness is created on the product's surface. Therefore, one of the ways to reduce the roughness factor and increase the product fatigue life is to control the relative slip and vibration between the cutting tool and the workpiece. To achieve this goal, the authors attempted to investigate the simultaneous effects of tool overhang and cutting depth on the static and dynamic deflection of the cutting tool in vitro. After that, the surface roughness was measured in different workpieces. Also, to study the high-cycle fatigue behavior of products with different surface roughness, four-point bending fatigue test was performed and stress-life diagram (S–N) was obtained. In addition, Basquin coefficients were extracted in terms of surface roughness. Eventually, the mathematical relationship between Basquin coefficients and surface roughness was presented by employing multiple linear regression (MLR) technique. This work was also done to obtain the relationship between machining parameters, including cutting depth and tool overhang, and surface roughness, and finally mathematical relation of life estimation was presented via the studied parameters. Next, S–N diagram of CK45 carbon steel considering surface roughness of 2.07 microns was predicted using the proposed model and different orders (first-, second-, and third-order regression). Comparison of the predicted data with the test results indicated that the mathematical model presented in this research is well able to evaluate the fatigue life of carbon steels with different roughness levels.

Keywords Tool overhang · Cutting depth · Tool deflections · Surface roughness · High-cycle fatigue behavior · S–N diagram

1 Introduction

In today's advanced world and competitive conditions, there are many manufacturers and mass production, which can offer higher quality products can be successful. In the manufacture of mechanical parts, two parameters of dimensional accuracy and surface roughness are considered quality variables. In the meantime, by performing several corrective and similar operations, the desired dimensions for the workpiece (observing the dimensional limitations in the assembly sets, based on the location constraints in different systems, and placing next to other parts) are achieved. But the parameter that is usually less important for the parts manufacturer is the surface roughness. This parameter depending on the performance of the component can be very important (e.g., in a shaft that is subjected to cyclic

✉ Siamak Ghorbani
gorbani_s@pfur.ru

[1] Department of Mechanical Engineering Technologies, Academy of Engineering, Peoples' Friendship University of Russia, RUDN University), 6 Miklukho-Maklaya Street, 117198 Moscow, Russian Federation

[2] Department of Transport, Academy of Engineering, Peoples' Friendship University of Russia, RUDN University), 6 Miklukho-Maklaya Street, 117198 Moscow, Russian Federation

[3] Mechanical Characteristics Lab, Center for Laboratory Services, Sharif University of Technology, Tehran 1458889694, Iran

loads, roughness has a significant impact on the service life of the system). Also, a sudden failure of the shaft can cause terrible damage to other parts of the system that work directly with the shaft, resulting in the failure of the entire system. In this regard, failure of the turbine blades can lead to the failure of all the blades due to collision and eventually damage to the central azis and failure of the turbine [1–3]. Therefore, the reliability, durability, and accuracy of the machines largely depend on the quality of surface treatment [4, 5]. Moreover, the main factors influencing the process of surface layer formation are the method of the cutting process, cutting conditions (i.e., cutting speed, feed rate, and cutting depth), tool overhang, cutting force, healthy technical and functional equipment, physical and mechanical characteristics of the workpiece, cutting properties and geometrical abilities of the cutting inserts, the rigidity of the technological system, damping ability, the availability and quality of lubricating, and cooling system [6, 7]. Also, the main parameters that determine the dynamic characteristics of the technological system are mass, the rigidity of the machine-device-cutting tool-workpiece, and its damping properties. In this regard, mass and stiffness are directly related to energy conservation and damping leads to energy loss in the system [8, 9]. To improve the dynamic characteristics of the technological system, which has a direct effect on the vibrational behavior of the system, the chatter phenomenon, and finally the surface quality of the product [10], it is necessary to increase their rigidity and damping properties as well as reduce their weight. In this regard, the damping capacity of a technological system is influenced by the cutting tool, machine, and workpiece [11, 12]. Practical experience shows that vibrations of the cutting tool during cutting operation occur at medium and high frequencies. Therefore, to ensure an accurate and efficient cutting process, it is necessary to reduce the oscillation of the cutting tool relative to the workpiece [13, 14]. According to the findings of researchers in this field, the reliability and performance of the cutting tool depend on the quality of the machining process (i.e., setting the appropriate values of process parameters). The efficiency of the cutting tool is characterized by durability, strength, rigidity, vibration resistance, stable chip crushing, and high productivity at the maximum permissible cutting conditions [15, 16]. In the meantime, settings of some important factors, such as technological equipment, cutting condition, workpiece, and material of cutting tool, are determined by the technological process, but tool overhang is the only parameter that is set arbitrarily [17, 18]. In addition, the tool overhang has a significant influence on the slip of cutting tool during operation and subsequently affects the surface quality (roughness). As it is stated by other scholars, during turning operation, including orthogonal and oblique cutting conditions, a large tool overhang may lead to the high vibration of the system and thus reduces the surface quality [19, 20]. On the other hand, effect of surface roughness as a quality parameter of the product has been investigated on the component performance under working conditions [21–26].

As mentioned before, shear force is one of the important parameters affecting product surface quality. This force acting on the chip formation from the tool side can be decomposed on the friction force (F) (which is along with the tool-chip interface) and normal force (N) (which is perpendicular to the friction force) as shown in Fig. 1a. In addition, there are shear force (F_s) and normal force to shear (F_N), which are applied by the workpiece on the chip. The shear force causes shear deformation to occur in the shear plane. These four forces (F, N, F_s, and F_N) vary with different cutting conditions and tool geometries; therefore, it is impossible to measure them [27]. However, chip formation during the cutting process takes place under the action of the cutting (F_c) and thrust (F_t) forces, which can be measured (Fig. 1b). The cutting force (F_c) is in the direction of cutting speed, and the thrust force (F_t) is perpendicular to the cutting force.

Exceeding the permissible stress values caused by these components significantly reduces the tool life, while, according to the working time, the tangential component has the greatest influence on the cutting insert, the increase in the values of which is directly related to the cross-sectional area of the layer being removed, that is, to the cutting depth [4, 6]. In addition, the occurrence of linear displacements of the cutting tool and, consequently, the quality of processing is influenced by harmful periodic mechanical vibrations

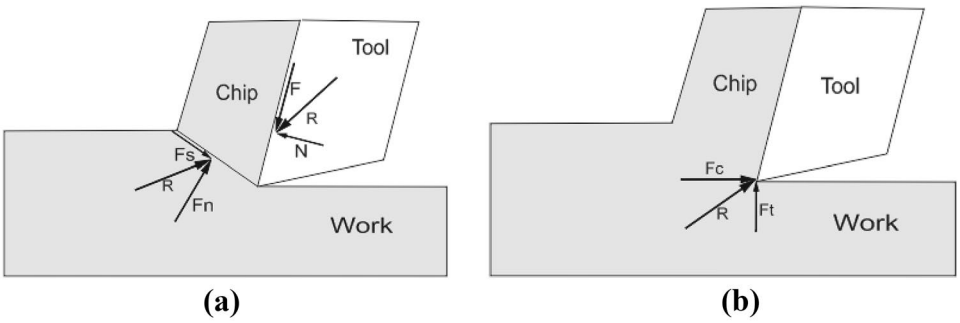

Fig. 1 **a** Cutting forces in orthogonal metal cutting applied by cutting tool and workpiece and **b** cutting force and thrust force acting on the tool which can be measured [27]

of the elastic body, which occur when the stability of the cutting process is lost. The elimination of this odious characteristic is associated with the correct installation of the cutting tool, namely, with the control of the size of the tool overhang from the tool holder within 1.5 times its holding height [15, 16]. If this requirement is not observed, vibrations are inevitable, which, as noted earlier, adversely affect the operation of the tool and, in addition to the occurrence of linear deformations of the tool holder, can lead to chip formation. Moreover, vibrations do not allow full control of the changes in cutting forces, as well as the nature of the loads that appeared during the cutting process, hence the need to reduce the cutting conditions to the detriment of quality, to keep the cutting force constant and bring the nature of the turning process as close as possible to the optimal one, and also reduce the likelihood of damage to the cutting tool and workpiece [17–19].

Cutting force, during turning operation, causes cutting tool deflection, which affects the stability of the system and surface quality of the product. Therefore, cutting tool condition monitoring plays an important role in turning operation. Extensive studies have been conducted on the characteristics of deviations in the loading process. Most of them tried to find a solution to this problem by identifying its causes and eliminating them. Ghorbani et al. have improved the static and dynamic characteristics of boring bars by proposing new boring bars with different cross sections [11]. In this research, the authors applied epoxy granite, which possesses high damping properties, in the structure of boring bars. They concluded that epoxy granite decreases the natural frequency of the boring bar and improves the surface quality of the part due to their better specific properties of strength and stiffness as well as high damping compared to steel and cast iron. Rogov and Ghorbani have used shims with different materials such as ceramic, epoxy granite, silty micaceous sandstone, granite, and chlorite schist to study the performance of the cutting tool on its static and dynamic characteristics [14]. The results of experiments have shown that the highest damping capacity and sufficient workability are achieved in the case of shims made of epoxy granite and silty micaceous sandstone. These shims suppress high-frequency vibrations, which can significantly improve the roughness quality by 20–40%. Gasagara et al. have experimentally and numerically analyzed tool vibration by proposing a new dynamic model of chatter phenomenon in terms of tool deflection [28]. The proposed model considers cutting forces, damping force, inertia force, and spring force. The authors claimed that tool deflection is the result of complex dynamic behavior (nonlinear interaction) between the cutting tool and workpiece. This causes chatter, which transits from periodic, quasi-periodic, and chaotic types. The experiment results showed that the machining stability decreases as feed rate and cutting depth increase. Wai and Suet have stated that for material with a low elastic modulus, the small displacement in the tool tip vibration on the machined surface causes secondary material swelling [29]. Therefore, an additional material pile-up on the machined surface is provided due to the secondary material swelling. This disturbs the assigned tool path and deteriorates the surface quality, which plays an important role, especially for a nanometric surface roughness formation. Also, a model of surface formation proposed by Wang et al. [30] considers the tool-tip vibration in ultra-precision diamond turning. They reported that the relative displacement between the cutting tool and workpiece during the turning process is a result of high-frequency tool-tip vibration. Chen and Zhao have evaluated the relative tool-work vibration suggesting a developed model, which contains cutting force, material property, and cutting parameters variations [31]. The obtained results showed that spindle speed is the most dominant factor affecting the relative vibration and the swelling effect in comparison with feed rate and cutting depth. It was also found that machining inhomogeneous materials causes higher relative tool-work vibration compared to a material with a homogeneous structure. According to the achievements of the study performed by Wang et al. [32], high-frequency tool-tip vibration with small amplitude is mainly caused by the tool–chip interface impact. They stated that surface roughness is mainly affected by the tool-tip vibration and the process damping effect. Lipski et al. have experimentally studied the effect of tool-workpiece vibrations, induced by random disturbances in a turning process, on the surface quality of the product [33]. They reported that large noise due to the higher amplitude in cutting force causes the tool-workpiece vibration. Kishore et al. have proposed and implemented a magnetorheological damper in a machine tool system to control cutting tool vibration in hard turning operation [34]. The proposed model is reduced cutting force and tool wears which led to the improvement of surface roughness. Ji et al. have demonstrated a new reacceptance coupling substructure analysis methodology which is proposed to predict the tool-tip dynamics [35]. In this way, they improved the prediction accuracy in the estimation of the reacceptance.

Thus, much research has been attempted to identify and suppress the cutting tool vibration by proposing different techniques. In addition, many efforts have been made to experimentally and numerically study the effect of surface roughness on the fatigue properties of various metals and alloys [36–39]. Also, in recent years, data mining and machine learning techniques such as neural network have been used to estimate the lifetime of metallic materials under cyclic loading conditions [40, 41]. Furthermore, in order to improve the fatigue life of metal parts, various surface treatment methods have been proposed, and the most efficient of them are different types of shot peening such as conventional shot peening (CSP), severe shot peening

(SSP), laser shock peening (LSP), and ultrasound shock peening (USP) [42–45]. However, they reported that shot peening treatment leads to increased surface roughness and irregularity and this has a negative effect on the fatigue life. But, superimposing the effects of this cold work on metallic parts is very beneficial from a fatigue viewpoint, and sometimes an increase of up to 2–8 times has been reported for fatigue strength. This statement is true in relation to the fatigue life in high regime that elastic deformation occurs during loading (the applied stress is less than the yield stress of the material). When there is plastic deformation during loading (i.e., the applied stress exceeds the material's yield stress), this statement is not true. In other words, SP treatment has a negative effect on the fatigue behavior of metals in the low cycle regime. It is better to say that the sensitivity to stress concentration caused by surface roughness in low-cycle fatigue is much higher than in high-cycle fatigue. Therefore, even with the application of mechanical operations with the aim of increasing the fatigue life, the level of surface roughness is of particular importance and should be considered in cases where several destructive phenomena are combined with each other, because its destructive effects are more than usual situation. Despite valuable researches done by scientists around the world so far, the industry still faces failures that after fracture analysis and failure study, it is determined that the main reason is fatigue phenomenon or its combination with other phenomena such as creep, hydrogen embrittlement, or corrosion. Therefore, it is necessary for the production of a part to consider not only the desired geometry as a criterion to determine the method of production and the use of that part; also, working conditions, load tolerance, surface quality, etc. must be considered (e.g., a component with a specific and not complex geometry may be produced by different methods, but each of them depends on the production method with mechanical properties and material defects and in sensitive cases, service life is also effective). Accordingly, in the present paper, the authors attempt to examine the simultaneous effects of tool overhang and depth of cut on vibration and tool deflection during static and dynamic loading in vitro. An abovementioned literature review showed that the cutting depth is the most effective turning process parameter (among the parameters of cutting depth, spindle speed, and feed rate) on the product quality like surface roughness. However, impact of tool overhang was rarely found. Therefore, the comprehensive study of the simultaneous effects of these two parameters was done by the authors for the first time, which is one of the most important innovations of this research. After that, the surface roughness of the parts is measured in terms of different tool overhang sizes, and finally their fatigue life is examined. Also, a new mathematical formulation were presented to assess high-cycle fatigue life of machined metallic components via size of tool overhang, which be able to predict lifetime with a good accuracy compared to the test results.

2 Materials

In this research, CK45 medium carbon steel was considered one of the most common and most widely used types of alloy steel in large and small industries. Despite the development of new materials as well as various alloys with special applications, this steel still has elements such as carbon, silicon (about 0.25%), and manganese (about 0.65%) with desirable properties such as impact resistance, tensile and compressive strength, fatigue properties, and high rigidity, and it is also suitable for various heat treatments. Other advantages of this steel include its availability and affordable price. Therefore, it has not been found a suitable alternative to this steel in various industries, including mechanical parts of heavy machinery (shafts, steering knuckle, and axles), petrochemicals, heavy industrial rollers, tillage tools, and hand tools such as hammers, pliers, and nails. The raw material has yield and ultimate stresses of 475 and 515 MPa, respectively, which was prepared as a rebar with a diameter of 50 mm. In addition, to ensure the purchase of raw material, quantum and tensile tests were performed so that all of them were in an acceptable range based on the steel key documentation.

2.1 Cutting tool

A Sandvik Coromant PCLNR 2525 M 12 right-hand lathe tool for external turning was selected as a cutting tool. This cutting tool has a replaceable insert made of T15K6 carbide alloy (insert CNMG 12 04 08–QM S205 (ANSI: CNMG 432–QM S205), the main cutting edge $\varphi = 95$ degrees, rake angle $\gamma = -6$ degrees, an inclination of the main blade $\lambda = -6$ degrees). The cutting tool, its dimension, and its accessories are shown in Fig. 2.

3 Experimental procedure

3.1 Measurement of cutting tool deflection

Cutting tool deflections were measured during static and dynamic loading of the cutting tool in different cutting depths ($t = 0.4,\ 1,$ and $1.5\ mm$). In the case of dynamic loading, the turning operation was performed on the lathe model 16K20 (manufacturer–StankoMashStroy (Russia)). Also, tool deflections were measured for different tool overhangs, including 35, 45, 55, 65, and 75 *mm*. It was outlined that the feed rate and spindle speed will not change throughout the experiment and will be taken equal to $s = 0.2\ mm/rev$ and $n = 1000\ rpm$,

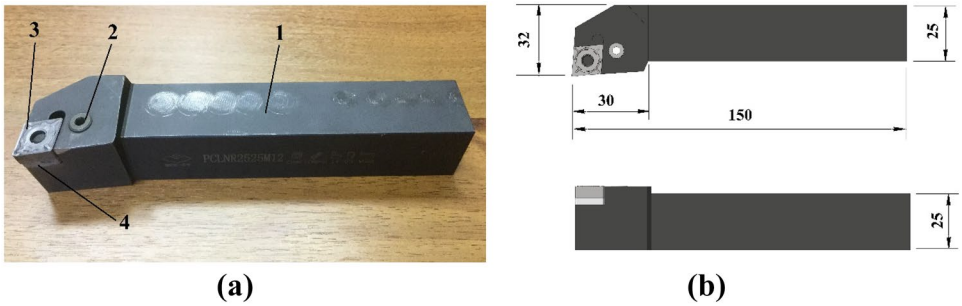

Fig. 2 **a** Cutting tool PCLNR2525M12 and its accessories, including 1, tool holder; 2, clamp screw; 3, cutting insert; and 4, shim. **b** Cutting tool's dimension (all dimensions are in millimeter)

respectively. Therefore, the actual cutting speed will be equal to $V_\phi = 155\ m/min$.

Chip formation during the cutting process is carried out under the action of the cutting force F_c, which is usually decomposed into components directed along the coordinate axes: tangential P_z, radial P_y, and axial P_x [6]. Cutting force was calculated using Eq. (1):

$$F_c = \sqrt{P_x^2 + P_y^2 + P_z^2} \tag{1}$$

where P_x is the axial cutting force. Also, P_y and P_z represent radial and tangential cutting forces, respectively.

Next, the cutting power was determined using Eq. (2) based on the corresponding cutting condition.

$$P_{cutting} = \frac{P_z.V_\phi}{1020.60} \tag{2}$$

where $P_{cutting}$ is the cutting power and V_ϕ represents actual cutting speed. In this regard, the revealed values of the cutting forces and cutting powers are presented in Table 1. The electric motor power of the machine main drive is equal to 10 kW.

The executive stage of the dynamic method included installation of the workpiece in a three-jaw self-centering chuck without tightening the rear center (this method of installation of the turned parts is characterized by vibrations arising in the contact area of the tool and workpiece) and installation of a dial indicator on the cross slide of the machine (Fig. 3a) so that its measuring tip touches the bottom of the cutting tool at a point roughly related to its tip. Next, the tool, which size of the tool holder is 25 × 25 mm, was fastened in the rotary tool holder by employing two M16 bolts. In the initial position, the indicator is set to zero, with a slight interference of 2–3 μm.

Table 1 Dependence of cutting force and power on the cutting depth

No.	Parameter	Value		
1	Cutting depth, mm	0.4	1.0	1.5
2	Cutting force, N	213	532	796
3	Cutting power, kW	0.5	1.2	1.8

During static loading, the cutting tool was loaded by different cutting forces (Table 1). The cutting forces were controlled by fixing them on a personal computer, which was connected to the tool tip. The resulting linear displacements were measured by the same indicator, installed in this case so that its measuring tip touches the cutting tool head at a point as close as possible to the plate (Fig. 3b). The cutting scheme is similar to the dynamic method; the overhang was changed by moving the tool holder fixed on the table. Additionally, due to the rearrangement of the set-up in the horizontal plane, the lever-type indicator determines the lateral shift. Figure 4 shows the loading device used in the static method [12, 20]. Loading of the cutting insert (part No. 2) of the cutting tool (part No. 1) was carried out by a cutting force simulation using a loading device (part No. 3) placed in a rack (part No. 4), fixed with four bolts on a plate (part No. 5). The loading device (part No. 3) is oriented relative to the cutting tool (part No. 1) so that the direction of application of the force by the rod (part No. 6) is cutting insert (part No. 2) coincided with the direction of the resultant cutting force. Also, magnitude controlling of the loading force was carried out using a dynamometer (part No. 8), which was an S-shaped strain gauge YZC-516c/VPG-36 (a full-bridge sensor that allows measuring the load of both compression and tension). In this case, the systematic error when connected via a 4-wire circuit can be compensated for calibrating the sensor. Also, additional temperature error can be considered insignificant, since all measurements were made in a room with a stable temperature and for a short time, which made it possible to avoid heating the load cells during operation. To convert the analog signal from the sensor to a discrete one, an Analog-to-Digital Converter (ADC) HX711 (part No. 9) connected to the computer was used: it has a 24-bit width and was used to convert the readings of strain gauges, scales, and force measurement sensors. The movement of the cutting head (part No. 2) was measured with an accuracy of 1 μm using two dial indicators in the vertical and horizontal planes (part No. 7). In the upper part of the rack (part No. 4), there is a bored hole in which the sleeve (part No. 10) of the loading device is located. Inside the sleeve (part No. 10), there is a quill (part No.

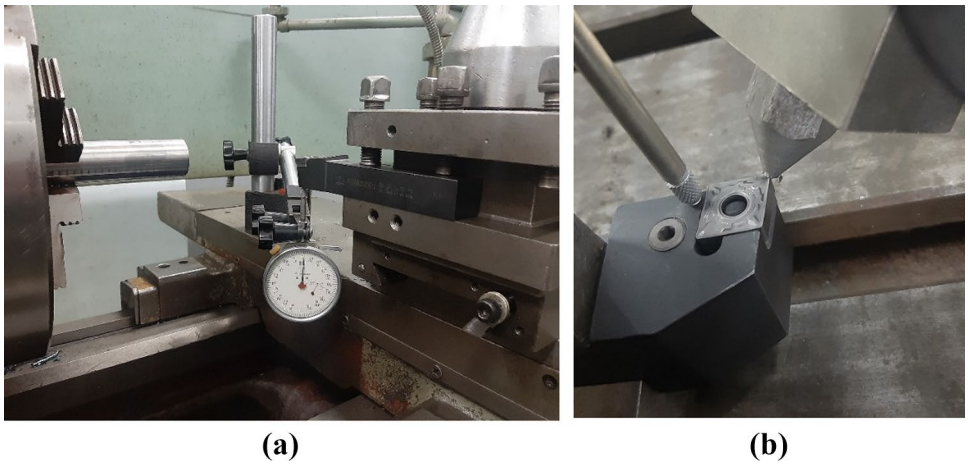

Fig. 3 Installation of the dial indicator in various experiments, including **a** dynamic method and **b** static method

11), which can be extended employing a screw (part No. 12) rotated by a handwheel (part No. 13). To reduce friction, the screw (part No. 12) is mounted on a thrust ball bearing (part No. 14). Together with the quill (part No. 11), the loading rod (part No.6) moves, transmitting the loading force to the cutting plate through the dynamometer (part No. 8).

3.2 Vibration measurement

To measure vibration, the cutting process was performed according to the conditions listed in Table 2. During turning operation, vibrations were measured using piezoelectric accelerometer KD-35 and employing ZETLAB software [11, 13]. To this end, as shown in Fig. 5, a piezoelectric accelerometer KD-35 is attached on the lower side of the tool tip, which records the vibration occurring during the cutting process. Then to visualize the results, a multifunctional spectrum analyzer A17-U8 pass recorded vibrations to a computer.

3.3 Surface roughness measurement

The main representation of the surface quality is the arithmetic mean deviation of the surface roughness profile (R_a) and mean roughness depth (R_z), since they have a great influence on the properties of the surface treatment [11, 13, 14]. In this study, the surface roughness of the workpiece was measured using a profilometer model 130. In this regard, the profilometer scans the irregularities of the measured surface by a diamond needle while moving along the measured surface and subsequent transformation of the resulting mechanical oscillations of the needle by an inductive sensor

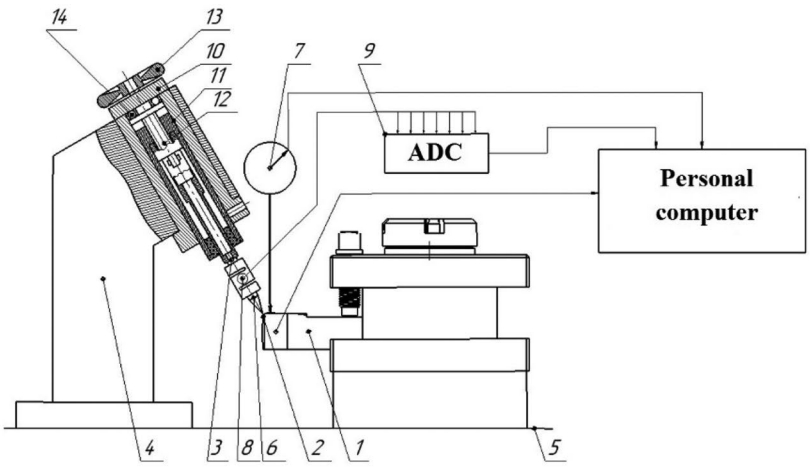

1 - Cutting tool
2 - Cutting insert
3 - Loading device
4 - Rack
5 - Plate
6 - Rod
7 - Dial indicator
8 - Dynamometer
9 - Analog-to-digital converter (ADC)
10 - Sleeve of the loading device
11 - Quill
12 - Screw
13 - Handwheel
14 - Thrust ball bearing

Fig. 4 Loading device accessories

Table 2 The cutting conditions aimed at measuring vibration

Parameter	Symbol	Unit	Value
Cutting depth	t	mm	1
Feed rate	S	mm/rev	0.2
Spindle speed	N	rpm	1000
Cutting speed	V	1/min	155
Cutting force	F_c	N	532
Cutting power	$P_{cutting}$	kW	1.2

into a measured signal. The sampling length was 12.50 mm and the measurement speed was 0.5 mm/s.

3.4 Rotating beam fatigue test

To investigate the high-cycle fatigue behavior of metallic materials and to obtain stress-life diagram (S–N), a rotary beam fatigue testing machine is usually used. Because this device is less expensive compared to axial fatigue devices and also due to the nature of this test, it is possible to perform tests with a high number of cycles due to the use of higher loading frequency compared to servo hydraulic devices in less time. In addition, this device operates with a fully reversed loading (i.e., constant stress ratio: $R = \frac{Min.\ loading}{Max.\ loading} = -1$) and no load changes occur during long-term tests. This device has three general modes of single-point bending, 3-point bending, and 4-point bending. In all of them, the sample rotates in a specific speed and proportional to the loading frequency. In single-point bending fatigue, a bending load is applied to the end of the specimen (rotating cantilever bending fatigue test based on the English standard BS3518 and known as Mac Adam Beam [46]). While in a three-point bending machine, a force is applied in the middle of the sample, and in a four-point bending machine, two parallel forces are applied with a distance of L from each other and $L/2$ from the center of the sample. To obtain a stress-life diagram in a high-cycle mode, it is necessary to perform fatigue tests considering at least 4 different stress levels [47, 48]. However, in order to more accurately assess the fatigue behavior of the material, 84 samples were prepared in accordance with ISO-1143 standard [49]. These samples were prepared according to the turning conditions mentioned in the previous step (7 different categories and 12 samples in each group). Also, in order to check the reliability and repeatability of the results, each test was performed twice and the average result was reported as the number of cycles to failure at that loading level. Thus, fatigue tests were performed in six different applied stresses in the range of 0.95 to 0.7 yield stress. Also, fatigue tests were performed with a loading frequency of 60 Hz at room temperature.

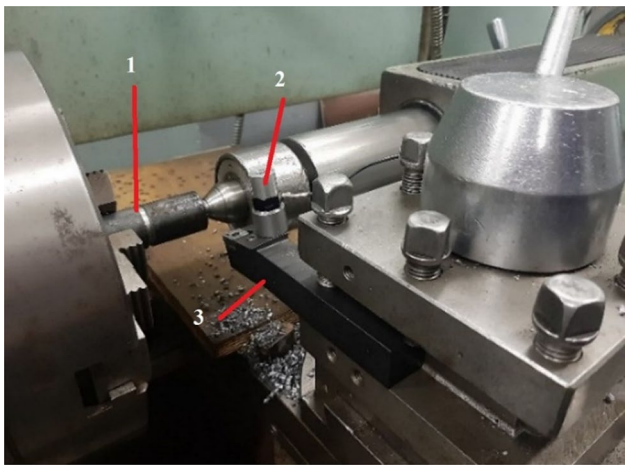

Fig. 5 Experimental set-up for vibration measurement, including 1, workpiece; 2, accelerometer KD-35; and 3, cutting tool

4 Results and discussion

4.1 Tool deflection

The results of static and dynamic deflection measurements as linear displacements are summarized in Table 3. The greatest linear deformation (40 μm) was detected at the 5th overhang and a cutting depth of $t = 1.5\ mm$.

Figure 6 illustrates the static and dynamic deflections vs. tool overhang-cutting force and tool overhang-cutting depth. From Fig. 6a, b, it is clear that the static and dynamic deflections increase by increasing the tool overhang and cutting force. Moreover, the sensitivity of the dynamic response to parameter changes is greater than that of the static response. However, for both case, the maximum value of dynamic deflection was observed in tool overhang of 75 mm and cutting force of 796 N. From Fig. 6c, d, as tool overhang and cutting depth increase, static and dynamic deflections of cutting tool also increase. In addition, for both case, the maximum value of dynamic deflection was observed in tool overhang and cutting force of 75 mm and 796 N, respectively. However, in the case of overhang of 35 mm, changing the cutting depth does not affect static deflection of cutting tool and is approximately equal to 1 µm. On the other hand, in the overhang of 35 mm, changing the cutting depth noticeably affects dynamic deflection of cutting tool (Table 3).

Table 3 Static and dynamic deflections of cutting tool based on experimental studies

Tool overhang, L, (mm)	Cutting depth, t (mm)	Cutting force, F_c (N)	Linear displacements (μm)		
			Static experiment		Dynamic deflection
			Static deflection	lateral shear	
35	0.4	213	0.98	0.97	6
	1.0	532	0.99	0.99	14
	1.5	796	1	0.98	21
45	0.4	213	0.50	0	7
	1.0	532	1.50	0.1	17
	1.5	796	2.50	0.1	25
55	0.4	213	0.50	0	10
	1.0	532	2.80	0	20
	1.5	796	5.00	0	30
65	0.4	213	0.40	0	15
	1.0	532	4.00	0	25
	1.5	796	6.80	0.1	36
75	0.4	213	0.50	0	18
	1.0	532	6.50	0	26
	1.5	796	11.50	0	40

4.2 Vibrations

The analysis results are presented in the form of narrow-band spectra (Fig. 7), which make it possible to determine the presence of tonal signals (discrete components) and noise components in the measuring channel by their shape. Furthermore, measurements were made when the tool overhang was equal to zero ($l = 0$). To this end, the vibration

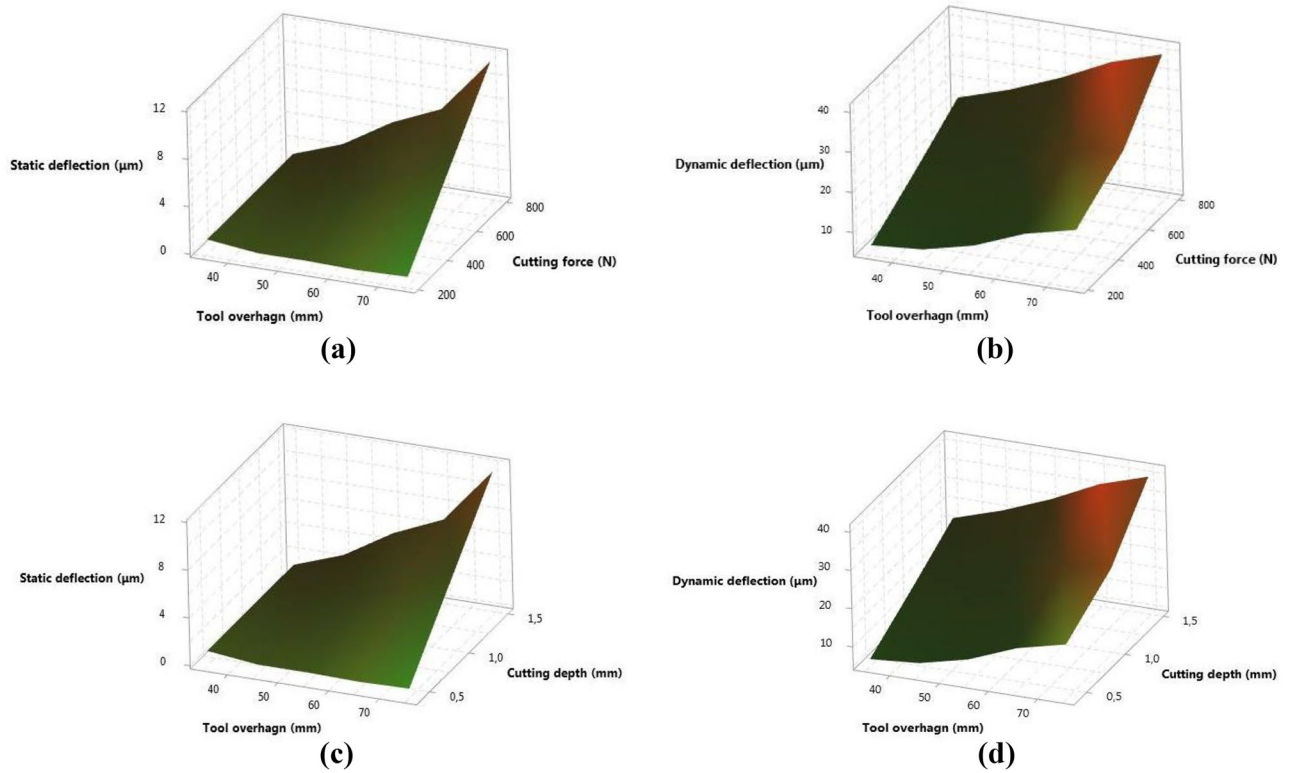

Fig. 6 Static and dynamic deflections vs. machining set-up parameters, including **a** static deflection in terms of tool overhang-cutting force, **b** dynamic deflection in terms of tool overhang-cutting force, **c** static deflection in terms of tool overhang-cutting depth, and **d** dynamic deflection in terms of tool overhang-cutting depth

sensor was installed on the cutting tool's head close to the cutting edge. To process the signals coming from the input channels of the spectrum analyzer modules, a narrow-band spectral analysis was used, in which the temporal realization of the signals was decomposed into the simplest components in the frequency domain (at the output, using the Fourier transform, a spectrum with an equal frequency step was obtained). Since the experimental part, as mentioned earlier, included a dynamic load on the cutting tool (the process is not stationary), then to identify the maximum values of the level of the received signals, the spectrogram sections were plotted in both time and frequency.

The data extracted from Fig. 7 was used to study the relationship between the vibration amplitude and tool overhang. In this regard, the variations of three statistical parameters, including the maximum, normal, and average values, in terms of tool overhang are displayed in Fig. 8. The results show that increasing the tool overhang leads to an increase the vibration amplitude (maximum values in the bar graph), which is associated with the fact that as tool overhang increases, the cutting tool's stiffness decreases. Eventually, this leads to a decrease in the dynamic stability of the system [11, 13, 14]. However, this relationship is not permanent, and it is clear that from tool overhang over 55 mm, the vibration amplitude converges to approximately 78.5 dB. Moreover, the results show that the mean vibration amplitude is almost constant (about 75 dB with a tolerance of 0.2 dB), indicating that changes in tool overhang settings during turning operation do not have an effect on the average tool vibration amplitude. In other words, the data collected indicate that this is a stationary process.

Next, the graphs of maximum and mean values of vibration amplitudes in frequency domain are obtained for all experimental cases using Mathcad Express Prime 4.0 (MEP = 4) as one of the well-known mathematical engineering software. Also, all graphs are superimposed on each other to optimize analytical work (Fig. 9).

4.3 Surface roughness

The profile of surface roughness for various tool overhangs is obtained and the main parameters of roughness (i.e., R_a and R_z) vs. tool overhang are depicted in Fig. 10. It is clear that both R_a and R_z increase by increasing the value of the tool overhang. This phenomenon is related to the fact that as the tool overhang increases, the dynamic stability of the system decreases (this interpretation is also evident in the results presented in Fig. 8). This increases the relative motion between the workpiece and the cutting tool affecting the quality of the machined surface [6, 50].

Next, it was tried to approximate the surface roughness of the machined component via tool overhang size by utilizing multilinear regression technique (polynomial function). As shown in Fig. 10, the accuracy of the approximation increases with increasing polynomial order (this accuracy is estimated by the coefficient of detection, which is usually $0< R^2 < 1$, and the closer value of this parameter to one indicates that the proposed function has a higher accuracy for detection). It is also observed that the fourth-order polynomial function has 100% predictablility. On the other hand, mathematics also expresses the fact that if there are n discrete data, it is necessary to use the polynomial function of degree $(n-1)$ to approximate them with the utmost accuracy. In this section, the surface roughness for five cases, including different tool overhangs, was examined and it was expected that regression by 4th-order polynomial function would have the best approximation, and this confirms the calculations performed at this stage.

4.4 Fatigue results

As noted in the literature review, surface roughness has a significant effect on the fatigue behavior of metals and acts like a stress concentration factor. However, these effects are not the same in different metals and should be checked separately for each material. Therefore, S–N diagrams as the results of fatigue test to identify the effect of surface roughness on the cyclic behavior of CK45 steel are shown in Fig. 11. From this figure, it is clear that as the surface roughness increases, the fatigue life decreases. Black color indicates the surface roughness defined in ISO-1143 standard and therefore the fatigue behavior of CK45 steel in these conditions was considered a criterion for comparing other conditions [51]. The results show that with increasing the level of applied stress, the fatigue behavior of the material is more sensitive to the surface quality (roughness). In other words, in very high-cycle fatigue regime, the effects of surface roughness are minimized. For example, at 450 and 330 MPa applied stresses for CK45 component with a surface roughness of 2.2 µm, the fatigue life reduction is about 38 and 34.7%, respectively, compared to the initial one (stated in the ISO standard). This is due to the fact that the surface roughness acts as a stress concentration and actually leads to the intensity of the stress at a certain point. Now, with increasing stress, there is a possibility that it will get bigger and go into the plastic deformation and low-cycle fatigue regime. Since the number of cycles to sample failure is very low in the LCF regime, the slightest change can have significant effects on the results. Now, by reducing the applied stress and considering the stress concentration coefficient corresponding to the surface roughness, the component remains in the high-cycle fatigue regime and the effects of this parameter are far less than the previous state. Finally, it can be concluded that if a sample made of CK45 steel with a surface roughness of approximately 2.22 µm is subjected

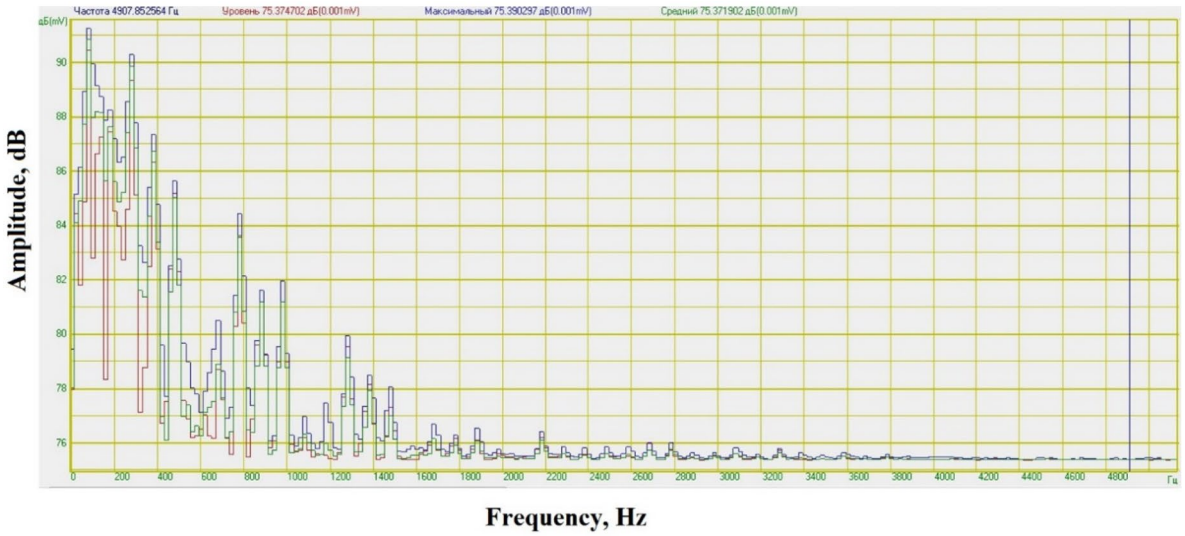

(a) Tool overhange of zero

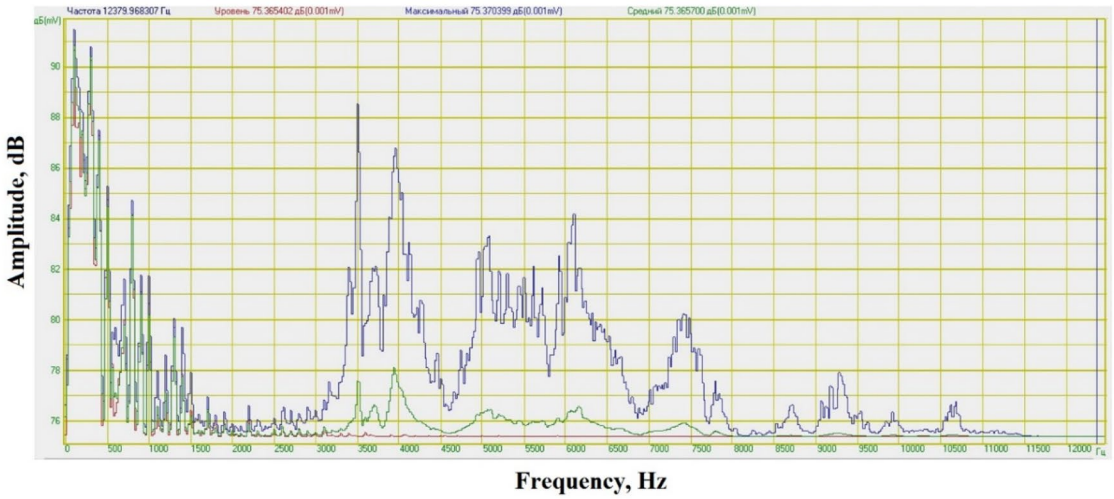

(b) Tool overhang of 35 mm

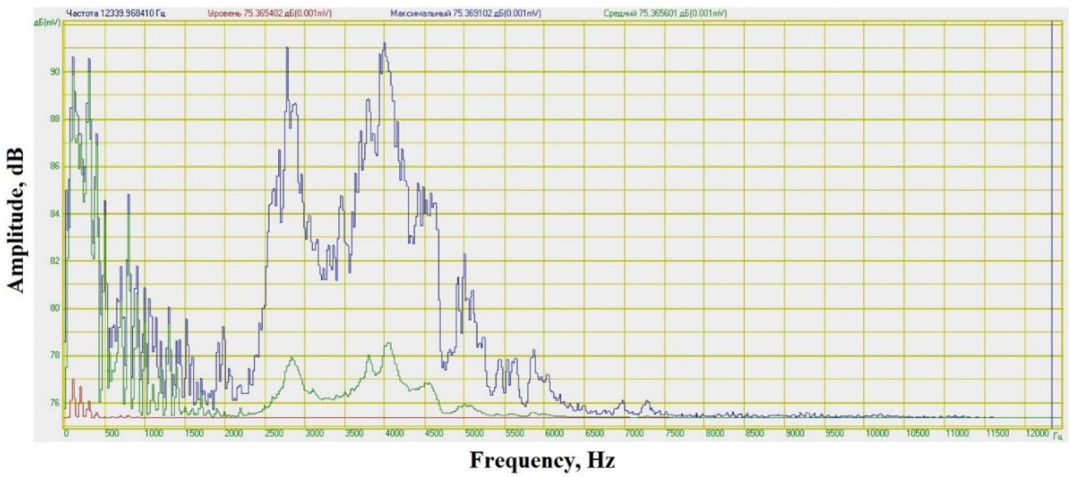

(c) Tool overhang of 45 mm

Fig. 7 Vibration amplitude variations in terms of frequency (narrowband spectrum in ZET-Lab) for various size of tool overhang, including **a** zero, **b** 35 mm, **c** 45 mm, **d** 55 mm, **e** 65 mm, and **f** 75 mm

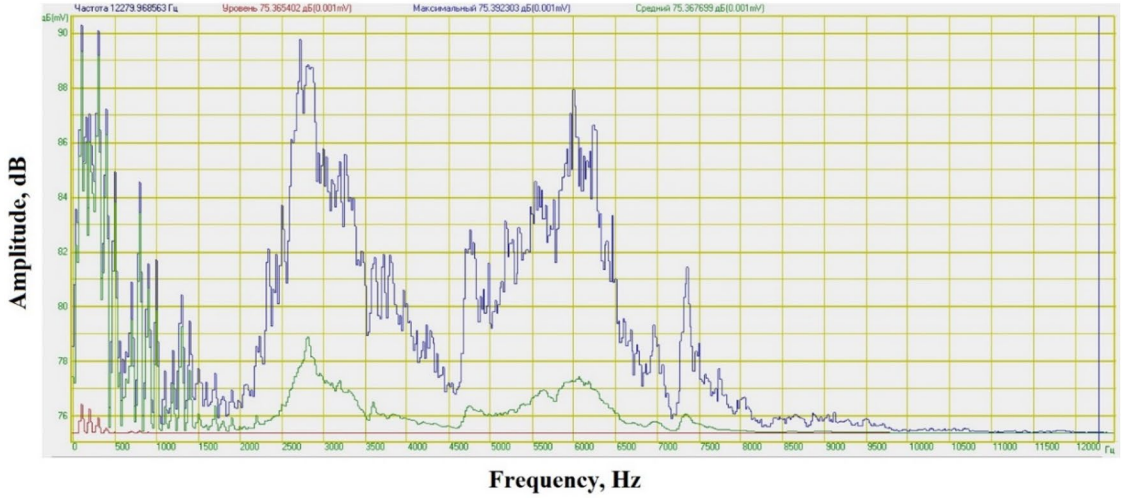

(d) Tool overhang of 55 mm

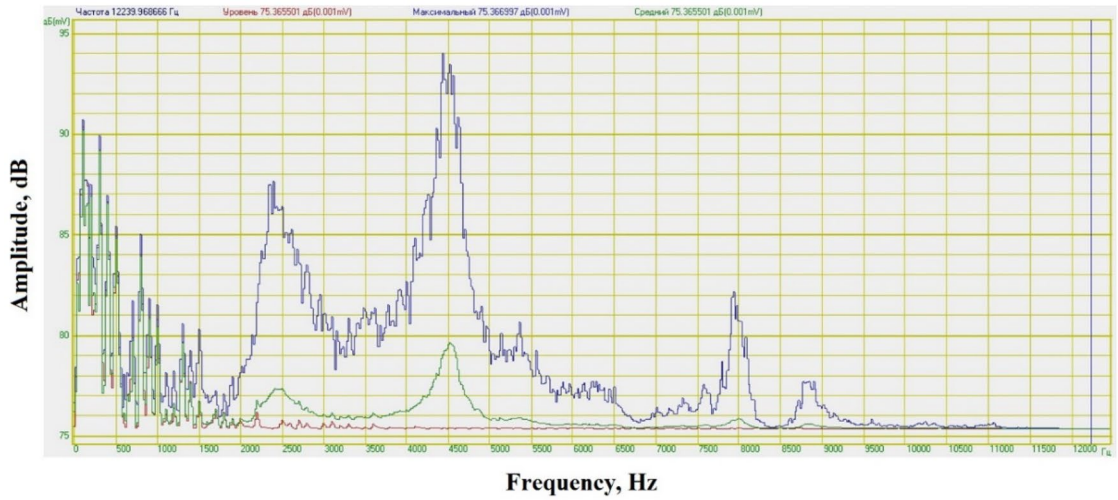

(e) Tool overhang of 65 mm

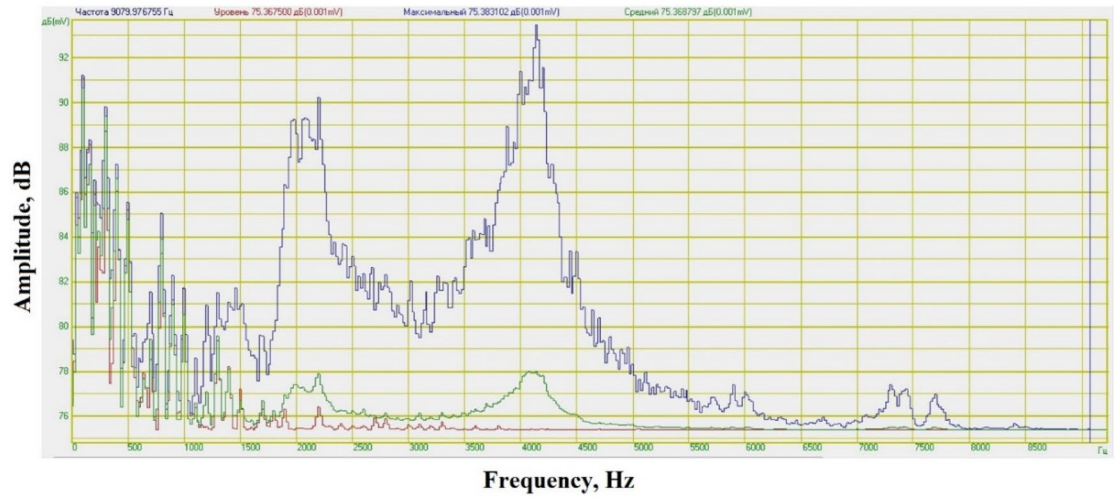

(f) Tool overhang of 75 mm

Fig. 7 (continued)

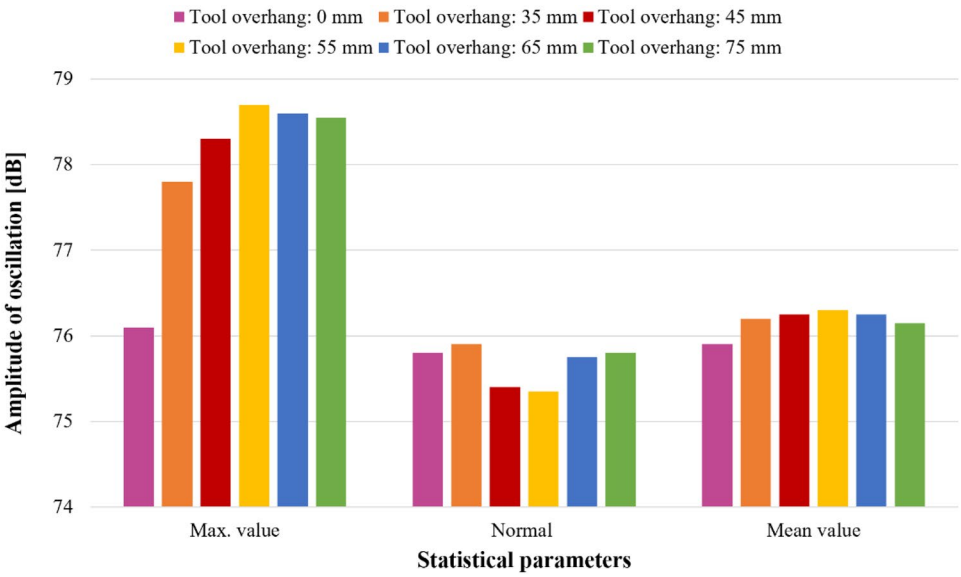

Fig. 8 The relationship between the amplitude of oscillations and tool overhang

to cyclic stresses less than 300 MPa, its fatigue life loss is far less than 34.7%.

Next, to extract the high-cycle fatigue (HCF) parameters, Basquin's equation was used as form of Eq. (3) [52]. This equation presents a linear relationship between the applied stress (S) and the number of cycles to failure in a log–log scale.

$$N = \frac{B}{(S)^m} \tag{3}$$

in which N represents number of cycles to failure, m is the slope of S–N diagram, and B is the value of the stress at one cycle. So, by specifying two points on the graph, the coefficients m and B can be obtained as follows:

$$m = \frac{\log(N_1) - \log(N_2)}{\log(S_2) - \log(S_1)} \tag{4}$$

$$B = N_1 \times (S_1)^m \tag{5}$$

Thus, using the experimental results (Fig. 11) and applying the above equations, the coefficients m and B for different cases of surface quality (roughness) are calculated and given in Table 4.

The coefficients obtained in this step show that by increasing surface roughness, both HCF parameters increase. Also, the intensity of this increasing trend decreases as the surface roughness of the machined component increases. Moreover, to provide a mathematical relationship for predicting HCF behavior of CK45 steel considering the desired surface roughness, multilinear regression method [53] was used. To achieve this purpose, a set of results is left unused to validate the new formula presented in the current research (the results of the randomly selected 2.07 level roughness were utilized in the next step). Also, in order to provide a more accurate and closer approximation to reality, different orders of linear regression were studied (first, second, and third order). The equations obtained to predict HCF parameters (i.e., Basquin's coefficients) in terms of surface roughness are as follows:

First-order linear regression:

$$m = 0.1770 \times R_a + 6.1939 \tag{6}$$

Second-order linear regression:

$$m = -0.06285 \times {R_a}^2 + 0.3252 \times R_a + 6.15175$$

Third-order linear regression:

$$m = -0.011 \times {R_a}^3 - 0.02 \times {R_a}^2 + 0.28 \times R_a + 6.160$$

First-order linear regression:

$$B = \left(3.089 \times R_a + 0.612\right)E + 21 \tag{7}$$

Second-order linear regression:

$$B = \left(-0.656 \times {R_a}^2 + 4.636 \times R_a + 0.172\right)E + 21$$

Third-order linear regression:

$$B = \left(-1.73 \times {R_a}^3 + 6.5 \times {R_a}^2 - 3.2 \times R_a + 1.47\right)E + 21$$

By replacing the surface roughness (2.07 μm) in Eqs. (6) and (7), the values of the Basquin's coefficients were calculated, and by employing Eq. (3), the fatigue life of CK45 steel with the desired roughness was predicted. The results

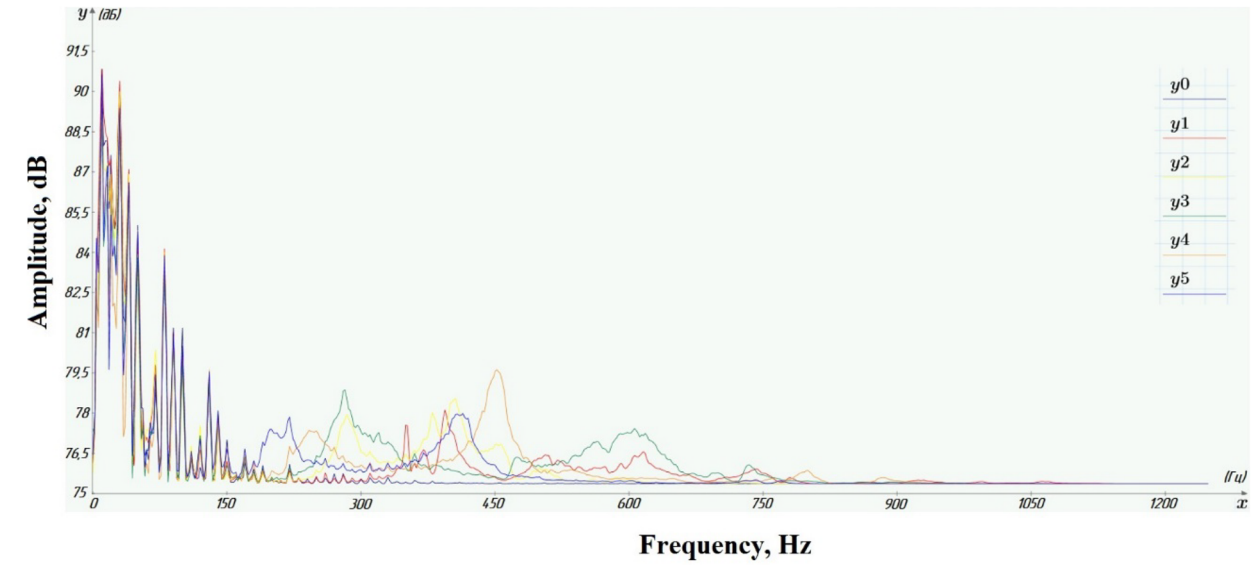

(a)

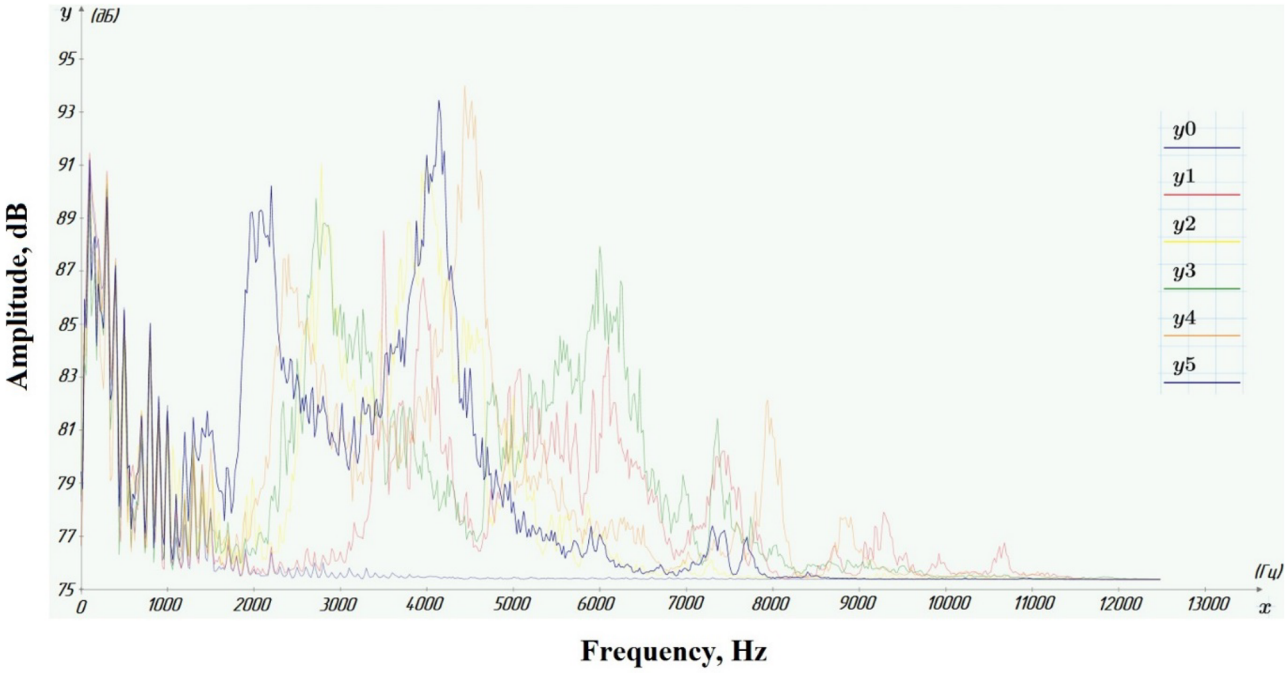

(b)

Fig. 9 Vibration amplitudes at various set up of tool overhang in terms of frequency, including **a** the mean values of the amplitudes and **b** the maximum values of the amplitudes in different cases, including y0 = 0 mm, y1 = 35 mm, y2 = 45 mm, y3 = 55 mm, y4 = 65 mm, and y5 = 75 mm

were compared with the experiment results (Fig. 12) to check the validity of the stated methodology.

From Fig. 12, it is clear that the relationships presented can well predict the high-cycle fatigue life of CK45 steel in terms of different surface roughness (maximum difference between predicted results and reality is less than 4%). Also, by using the 4th-order polynomial function as surface roughness according to the size of tool overhang in the turning operation mentioned in this research and its placement in the proposed fatigue relations, the fatigue life of CK45 steel can be dependent on the size of tool overhang in the settings of turning operations (Eq. (8)).

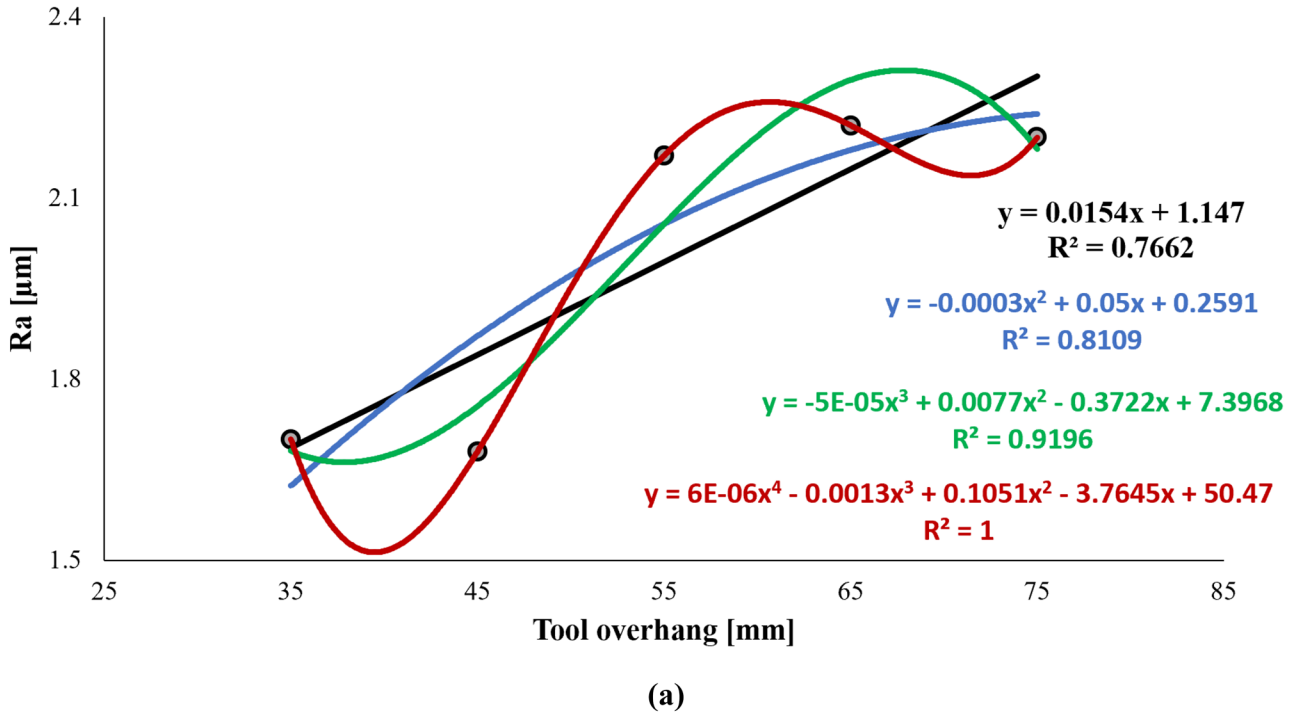

(a)

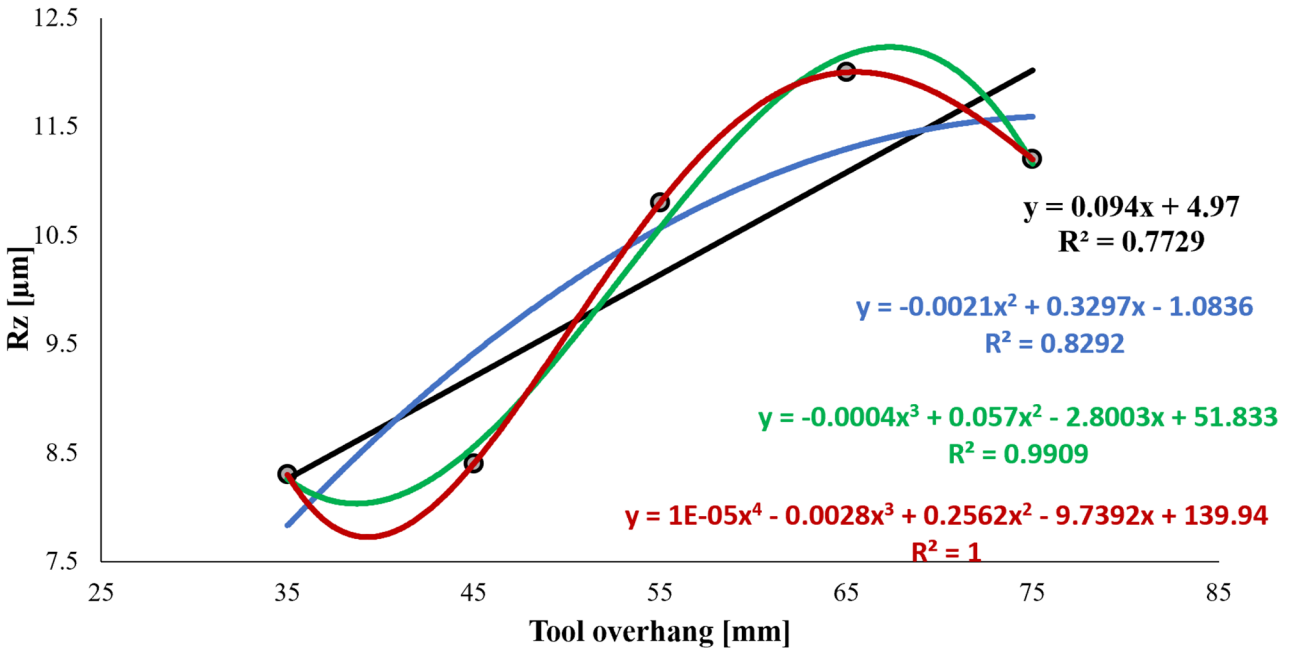

(b)

Fig. 10 The results of surface roughness measurements for all cases to extract the relationship between different parameters of surface roughness and tool overhang, including **a** arithmetical mean roughness value: R_a and **b** mean roughness depth: R_z

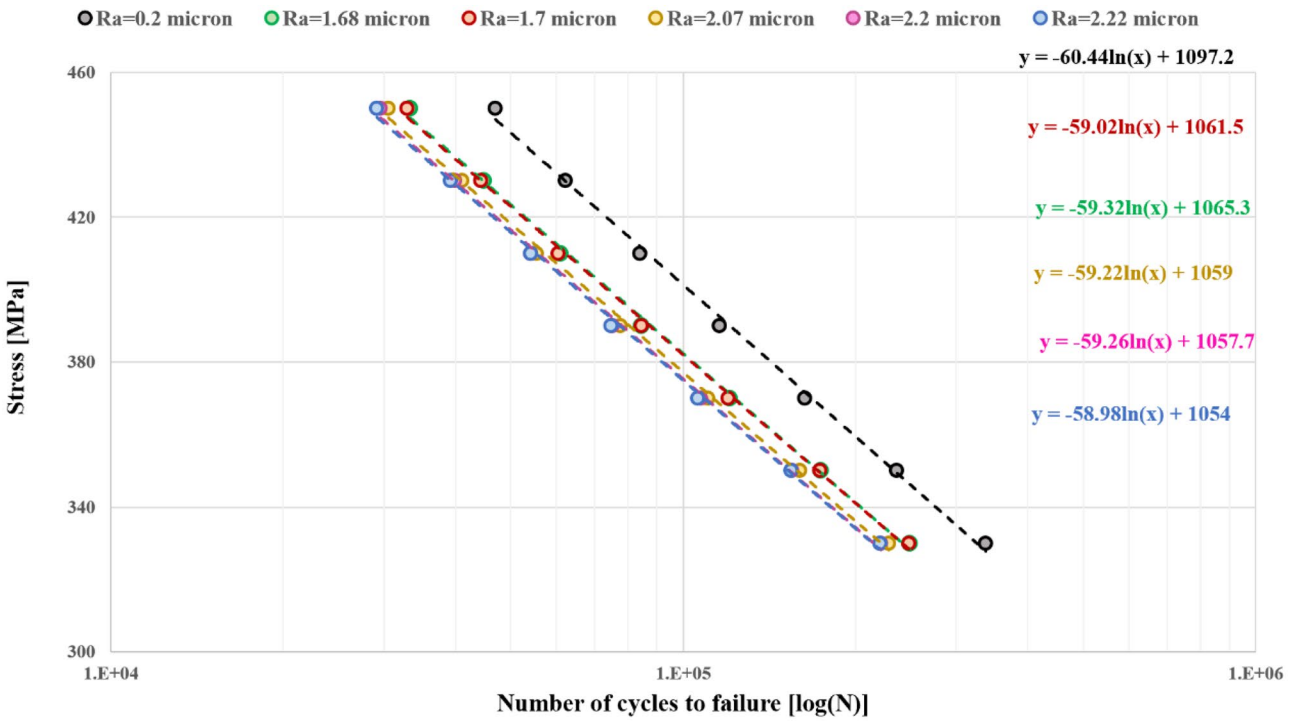

Fig. 11 The S–N diagrams of CK45 steel with different surface quality: experimental data

$$N = \frac{\left(-1.73 \times {R_a}^3 + 6.5 \times {R_a}^2 - 3.2 \times R_a + 1.47\right)E + 21}{(S)^{-0.011 \times {R_a}^3 - 0.02 \times {R_a}^2 + 0.28 \times R_a + 6.160}} \tag{8}$$

where

$$R_a = 6E - 06 \times l^4 - 0.0013 \times l^3 + 0.1051 \times l^2 - 3.7645 \times l + 50.47 \tag{9}$$

Finally, the formulation obtained from substituting Eq. (9) into the Eq. (8) can be used to estimate the fatigue life of the CK45 part in terms of size of tool overhang in the turning process.

As it is clear, the Basquin equation for the high-cycle region is presented as a linear relationship. Also, the results of this research showed that there is no linear relationship between roughness and fatigue life, and the sensitivity to roughness is much higher in the low-cycle fatigue regime, so there is a non-linear relationship between these two variables (roughness and cyclic lifetime). Since the focus of this article is on HCF behavior and the S–N region without plastic deformation, therefore, this relationship can be assumed to be linear with great accuracy. On the other hand, for the first time in this research, the relationship between the size of tool overhang and the roughness caused by the turning process was investigated experimentally, and according to Fig. 10, there is no linear relationship. But since there is only one independent parameter, linear regression technique was used and there will be no interaction between the variables. Therefore, by considering the highest order in this approximation, the highest accuracy was achieved, and finally, by combining the abovementioned achievements, a novel mathematical formulation was presented, which is able to adjust the tool overhang parameter in turning process based on the desired fatigue life of the CK45 component. Eventually, this can be done for other metals and a table of correction factors can be obtained for each material. In this way, artisans can improve the quality and efficiency of their products from the fatigue viewpoint.

Table 4 The HCF parameters of CK45 steel considering different surface roughness (Basquin's coefficients)

Surface roughness (μm)	m	B
0.2	6.214279973	1.07327E+21
1.68	6.517705587	6.00283E+21
1.7	6.526201039	6.2704E+21
2.07	6.550291485	6.85922E+21
2.2	6.560803226	7.14101E+21
2.22	6.566031396	7.28212E+21

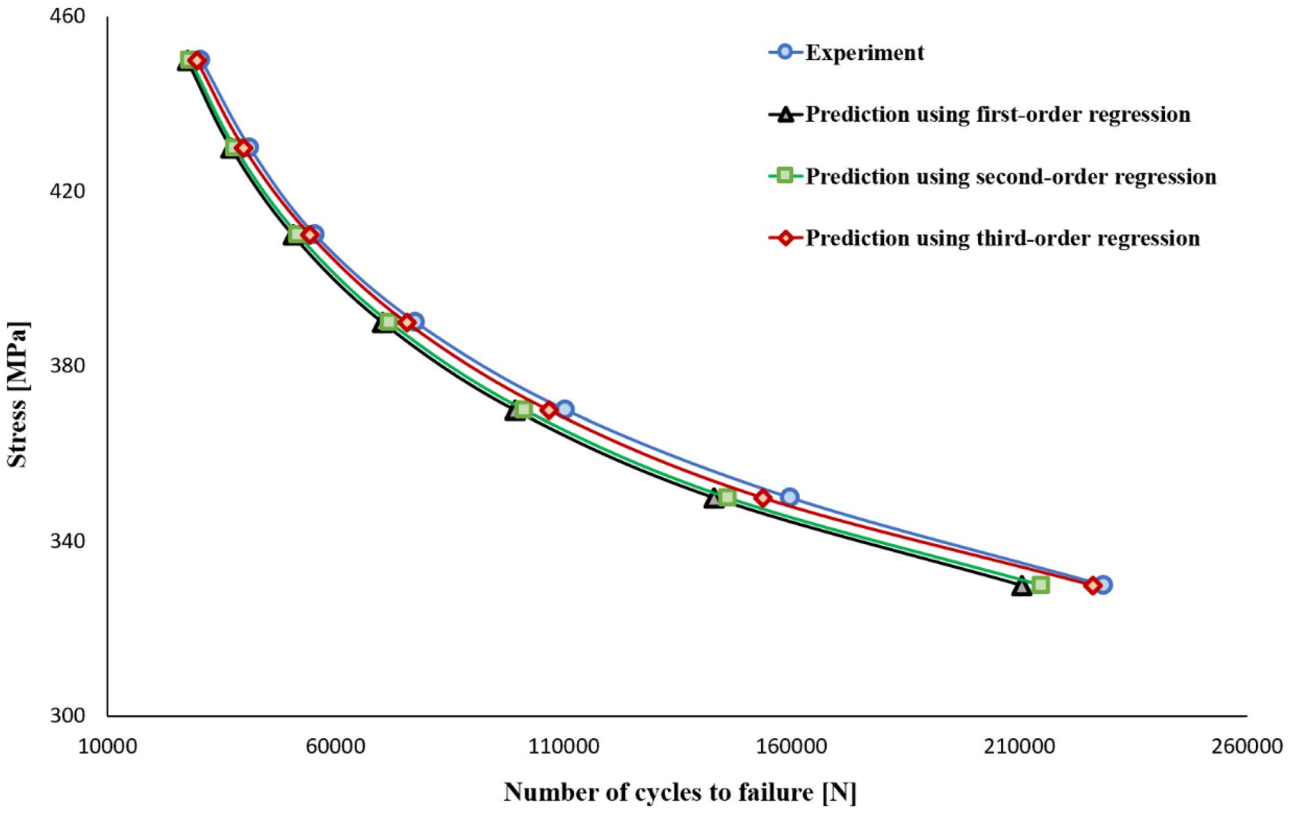

Fig. 12 Comparison of predicted fatigue behavior of CK45 steel considering the surface roughness of 2.07 μm with experiment results

5 Conclusions

The current paper studied experimentally the simultaneous influence of cutting depth and tool overhang on the dynamic and static tool deflection, vibrations, surface quality, and high-cycle fatigue properties of CK45 steel. As a result of the study it was revealed that:

- Static and dynamic deflections of cutting tool increase as tool overhang and cutting depth increase. Also, the dynamic response is more sensitive to parameters' variations than the static response.
- Increasing the tool overhang leads to increase the maximum values of vibration amplitude, which is related to the decreased cutting tool's stiffness, and as the tool overhang increases, both roughness parameters (R_a & R_z) increase due to the unstable dynamic system.
- LCF behavior of the material is more sensitive to the surface quality compared to HCF behavior, which is related to the fact that the surface roughness acts as a stress concentration leading to the intensity of the stress at a certain point.
- The results indicated that by increasing surface roughness, both Basquin's coefficients increase. Moreover, the intensity of this increasing trend decreases as the surface roughness of the machined component increases.
- The most important achievement of this research includes the proposal of a new mathematical relationship to adjust the size of tool overhang with the aim of achieving the desired fatigue strength in the turned CK45 component.
- Comparing the results obtained from the proposed new formula with the experimental data shows a difference of 4%, which shows the good accuracy of this methodology for adjusting the size of tool overhang in the turning process.

Acknowledgements This paper has been supported by the RUDN University Strategic Academic Leadership Program.

Author contribution Dmitry Gennadievich Allenov: conceptualization, investigation, data analysis, experiments, and writing–original draft preparation. Kristina Deinova Borisovna: data analysis, investigation, experiments, and writing–original draft preparation. Siamak Ghorbani: investigation, data analysis, experiments, and writing–reviewing and editing. Kazem Reza Kashyzadeh: conceptualization, investigation, data analysis, experiments, fatigue section, and writing–reviewing and editing.

Availability of data and material All the data have been presented in the manuscript.

Code availability Not applicable.

Declarations

Ethics approval The authors state that the present work is in compliance with the ethical standards.

Consent to participate The authors declare that they all consent to participate in this research.

Consent for publication The authors declare that they all consent to publish the manuscript.

Competing interests The authors declare no competing interests.

References

1. Carter TJ (2005) Common failures in gas turbine blades. Eng Fail Anal 12(2):237–247. https://doi.org/10.1016/j.engfailanal.2004.07.004
2. Farrahi GH, Tirehdast M, Abad EMK, Parsa S, Motakefpoor M (2011) Failure analysis of a gas turbine compressor. Eng Fail Anal 18(1):474–484. https://doi.org/10.1016/j.engfailanal.2010.09.042
3. Fahmi ATWK, Kashyzadeh KR, Ghorbani S (2022) A comprehensive review on mechanical failures cause vibration in the gas turbine of combined cycle power plants. Eng Fail Anal 134:106094. https://doi.org/10.1016/j.engfailanal.2022.106094
4. Siddhpura M, Paurobally R (2012) A review of chatter vibration research in turning. Int J Mach Tools Manuf 61:27–47. https://doi.org/10.1016/j.ijmachtools.2012.05.007
5. Daghini L (2012) Improving machining system performance through designed-in damping: modelling, analysis and design solutions. Dissertation, KTH Royal Institute of Technology
6. Thomas C, Katsuhiro M, Toshiyuki O, Yasuo Y (2000) Metal machining: Theory and applications. Arnold Publisher, Great Britain
7. Rogov VA, Ghorbani S (2015) Research on selecting the optimal design of antivibrational lathe tool using computer simulation. Proc Inst Mech Eng Eng-J Pro 229(3):162–167. https://doi.org/10.1177/0954408913513450
8. Kozochkin MP, Volosova MA, Allenov DG (2016) Effect of wear of tool cutting edge on detail surface layer deformation and parameters of vibro-acoustic signals. Mater Sci Forum 876:50–58. https://doi.org/10.4028/www.scientific.net/MSF.876.50
9. Allenov D, Deinova K, Konoplev V, Korzin A (2019) Effect of fixing the pass-through turning tool in the tool holder on the roughness and surface macro deflections during turning. IOP Conf Ser Mater Sci Eng 675:012046. https://doi.org/10.1088/1757-899X/675/1/012046
10. Kashyzadeh KR, Ostad-Ahmad-Ghorabi MJ (2012) Study of chatter analysis in turning tool and control methods–a review. Int J Emerg Technol Adv 2(4):1–5
11. Ghorbani S, Rogov VA, Carluccio A, Belov PS (2019) The effect of composite boring bars on vibration in machining process. Int J Mach Tools Manuf 105:1157–1174. https://doi.org/10.1007/s00170-019-04298-6
12. Ghorbani S, Kopilov VV, Polushin NI, Rogov VA (2018) Experimental and analytical research on relationship between tool life and vibration in cutting process. Arch Civ Mech 18(3):844–862. https://doi.org/10.1016/j.acme.2018.01.007
13. Rogov VA, Ghorbani S, Popikov AN, Polushin NI (2017) Improvement of cutting tool performance during machining process by using different shim. Arch Civ Mech 17(3):694–710. https://doi.org/10.1016/j.acme.2017.01.008
14. Rogov VA, Ghorbani S (2014) The effect of tool construction and cutting parameters on surface roughness and vibration in turning of AISI 1045 steel using Taguchi method. MME 4:8–18. https://doi.org/10.4236/mme.2014.41002
15. Kiyak M, Kaner B, Sahin I, Aldemir B, Cakir O (2010) The dependence of tool overhang on surface quality and tool wear in the turning process. Int J Mach Tools Manuf 51(5):431–438. https://doi.org/10.1007/s00170-010-2654-y
16. Song Q, Shi J, Liu Z, Wan Y, Xia F (2016) Boring bar with constrained layer damper for improving process stability. Int J Mach Tools Manuf 83(9):1951–1966. https://doi.org/10.1007/s00170-015-7670-5
17. Clancy BE, Shin YC (2002) A comprehensive chatter prediction model for face turning operation including tool wear effect. Int J Mach Tools Manuf 42(9):1035–1044. https://doi.org/10.1016/S0890-6955(02)00036-6
18. Haddadi E, R Shabgha M, Ettefag M (2008) Effect of different tool edge conditions on wear detection by vibration spectrum analysis in turning operation. J Appl Sci 8(21):3879–3886. https://doi.org/10.3923/jas.2008.3879.3886
19. Taşdemir Ş, Neşeli S, Saritaş I, Yaldiz S (2008) Prediction of surface roughness using artificial neural network in lathe. In Proceedings of the 9th International Conference on Computer Systems and Technologies and Workshop for PhD Students in Computing 08:IIIB.6–1–IIIB.6–8. https://doi.org/10.1145/1500879.1500925
20. Kopylov VV (2002) Development and research of experimental-analytical model of interrelation of durability of prefabricated passing cutting tools with parameters of their oscillations in cutting process. Dissertatin, Experimental Research Institute of Metal-Cutting Machine Tools.Moscow, Russia
21. Lai WJ, Ojha A, Luo Z (2022) Effect of surface roughness on fatigue behavior of 316L stainless steel produced by binder jetting process. In: TMS 2022 151st Annual Meeting & Exhibition Supplemental Proceedings. Springer, Cham, pp 164–176. https://doi.org/10.1007/978-3-030-92381-5_15
22. Quan F, Chen Z, Ye H, Cui C, Cui Y (2021) Study of the effect of surface roughness on fatigue strength of GH4169 based on indirect evaluation of the notch root radius. Int J Fatigue 152:106440. https://doi.org/10.1016/j.ijfatigue.2021.106440
23. Khisheh S, Khalili K, Azadi M, Hendouabadi VZ (2021) Influences of roughness and heat treatment on high-cycle bending fatigue properties of A380 aluminum alloy under stress-controlled cyclic loading. Mater Chem Phys 264:124475. https://doi.org/10.1016/j.matchemphys.2021.124475
24. Jinlong W, Wenjie P, Jing Y, Jingsi W, Mingchao D, Yuanliang Z (2021) Effect of surface roughness on the fatigue failure and evaluation of TC17 titanium alloy. Mater Sci Technol 37(3):301–313. https://doi.org/10.1080/02670836.2021.1885777
25. Wang H, Liu X, Wu Q, Wang X, Wang Y (2021) An improved fatigue life prediction model for shock absorber cylinder with surface roughness correction. Eng Comput 38(6):2713–2732. https://doi.org/10.1108/EC-05-2020-0263
26. Lee S, Rasoolian B, Silva DF, Pegues JW, Shamsaei N (2021) Surface roughness parameter and modeling for fatigue behavior of additive manufactured parts: a non-destructive data-driven approach. Addit Manuf 46:102094. https://doi.org/10.1016/j.addma.2021.102094
27. Rodríguez PJM (2014) Numerical modeling of metal cutting processes using the particle finite element method. Dissertation, Universitat Politècnica de Catalunya (UPC). http://hdl.handle.net/10803/145692
28. Gasagara A, Jin W, Uwimbabazi A (2019) Stability analysis for a single-point cutting tool deflection in turning operation. Adv Mech Eng 11(6):1–14. https://doi.org/10.1177/1687814019853188
29. Yip WS, To S (2019) Theoretical and experimental investigations of tool tip vibration in single point diamond turning of

titanium alloys. Micromachines 10(4):231. https://doi.org/10.3390/mi10040231
30. Wang H, To S, Chan CY (2013) Investigation on the influence of tool-tip vibration on surface roughness and its representative measurement in ultra-precision diamond turning. Int J Mach Tools Manuf 69:20–29. https://doi.org/10.1016/j.ijmachtools.2013.02.006
31. Chen J, Zhao Q (2015) A model for predicting surface roughness in single-point diamond turning. Measurement 69:20–30. https://doi.org/10.1016/j.measurement.2015.03.004
32. Wang H, To S, Chan CY, Cheung CF, Lee WB (2010) A theoretical and experimental investigation of the tool-tip vibration and its influence upon surface generation in single-point diamond turning. Int J Mach Tools Manuf 50(3):241–252. https://doi.org/10.1016/j.ijmachtools.2009.12.003
33. Lipski J, Litak G, Rusinek R, Szabelski K, Teter A, Warmiński J, Zaleski K (2002) Surface quality of a work material's influence on the vibrations of the cutting process. J Sound Vib 252(4):729–737. https://doi.org/10.1006/jsvi.2001.3943
34. Kishore R, Choudhury SK, Orra K (2018) On-line control of machine tool vibration in turning operation using electro-magneto rheological damper. J Manuf Process 31:187–198. https://doi.org/10.1016/j.jmapro.2017.11.015
35. Ji Y, Bi Q, Zhang S, Wang Y (2018) A new receptance coupling substructure analysis methodology to predict tool tip dynamics. Int J Mach Tools Manuf 126:18–26. https://doi.org/10.1016/j.ijmachtools.2017.12.002
36. Nakatani M, Masuo H, Tanaka Y, Murakami Y (2019) Effect of surface roughness on fatigue strength of Ti-6Al-4V alloy manufactured by additive manufacturing. Procedia Struct Integr 19:294–301. https://doi.org/10.1016/j.prostr.2019.12.032
37. Pegues J, Roach M, Williamson RS, Shamsaei N (2018) Surface roughness effects on the fatigue strength of additively manufactured Ti-6Al-4V. Int J Fatigue 116:543–552. https://doi.org/10.1016/j.ijfatigue.2018.07.013
38. Lai J, Huang H, Buising W (2016) Effects of microstructure and surface roughness on the fatigue strength of high-strength steels. Procedia Struct Integr 2:1213–1220. https://doi.org/10.1016/j.prostr.2016.06.155
39. Bayoumi MR, Abdellatif AK (1995) Effect of surface finish on fatigue strength. Eng Fract Mech 51(5):861–870. https://doi.org/10.1016/0013-7944(94)00297-U
40. Maleki E, Unal O, Kashyzadeh KR (2018) Fatigue behavior prediction and analysis of shot peened mild carbon steels. Int J Fatigue 116:48–67. https://doi.org/10.1016/j.ijfatigue.2018.06.004
41. Maleki E, Unal O, Kashyzadeh KR (2018) Effects of conventional, severe, over, and re-shot peening processes on the fatigue behavior of mild carbon steel. Surf Coat Technol 344:62–74. https://doi.org/10.1016/j.surfcoat.2018.02.081
42. Maleki E, Unal O, Reza Kashyzadeh K (2019) Efficiency analysis of shot peening parameters on variations of hardness, grain size and residual stress via Taguchi approach. Met Mater Int 25(6):1436–1447. https://doi.org/10.1007/s12540-019-00290-7
43. Maleki E, Unal O, Kashyzadeh KR (2019) Surface layer nanocrystallization of carbon steels subjected to severe shot peening: analysis and optimization. Mater Charact 157:109877. https://doi.org/10.1016/j.matchar.2019.109877
44. Maleki E, Unal O, Kashyzadeh KR, Bagherifard S, Guagliano M (2021) A systematic study on the effects of shot peening on a mild carbon steel: microstructure, mechanical properties, and axial fatigue strength of smooth and notched specimens. Appl Surf Sci Adv 4:100071. https://doi.org/10.1016/j.apsadv.2021.100071
45. Maleki E, Farrahi GH, Reza Kashyzadeh K, Unal O, Gugaliano M, Bagherifard S (2021) Effects of conventional and severe shot peening on residual stress and fatigue strength of steel AISI 1060 and residual stress relaxation due to fatigue loading: experimental and numerical simulation. Met Mater Int 27(8):2575–2591. https://doi.org/10.1007/s12540-020-00890-8
46. Maleki E, Reza Kashyzadeh K (2017) Effects of the hardened nickel coating on the fatigue behavior of ck45 steel: experimental, finite element method, and artificial neural network modeling. J Mater Sci Eng 14(4):81–99. https://doi.org/10.22068/ijmse.14.4.81
47. Arghavan A, Reza Kashyzadeh K, Amiri Asfarjani A (2011) Investigating effect of industrial coatings on fatigue damage. Appl Mech Mater 871:230–237. https://doi.org/10.4028/www.scientific.net/amm.87.230
48. Kashyzadeh KR, Arghavan A (2013) Study of the effect of different industrial coating with microscale thickness on the CK45 steel by experimental and finite element methods. Strength Mater 45:748–757. https://doi.org/10.1007/s11223-013-9510-x
49. ISO 1143 (2021) Metallic materials – Rotating bar bending fatigue testing
50. Kashyzadeh KR, Ghorbani S (2020) Numerical study of free vibration behaviour of filled tool holder using epoxy-granite. J Phys Conf Ser 1687(1):012025. https://doi.org/10.1088/1742-6596/1687/1/012025
51. Reza Kashyzadeh K, Maleki E (2017) Experimental investigation and artificial neural network modeling of warm galvanization and hardened chromium coatings thickness effects on fatigue life of AISI 1045 carbon steel. J Fail Anal Prev 17(6):1276–1287. https://doi.org/10.1007/s11668-017-0362-8
52. Stephens RI, Fatemi A, Stephens RR, Fuchs HO (2000) Metal fatigue in engineering. John Wiley & Sons
53. Farrahi GH, Kashyzadeh KR, Minaei M, Sharifpour A, Riazi S (2020) Analysis of resistance spot welding process parameters effect on the weld quality of three-steel sheets used in automotive industry: experimental and finite element simulation. IJE 33(1):148–157. https://doi.org/10.5829/ije.2020.33.01a.17